

Old Dominion University ODU Digital Commons

Bioelectrics Publications

Frank Reidy Research Center for Bioelectrics

10-2017

Activation of the Phospholipid Scramblase TMEM16F by Nanosecond Pulsed Electric Field (nsPEF) Facilitates Its Diverse Cytophysiological Effects

Claudia Muratori

Old Dominion University, cmurator@odu.edu

Andrei G. Pakhomov

Old Dominion University, apakhomo@odu.edu

Elena Gianulis

Old Dominion University


Jade Meads

Old Dominion University

Maura Casciola

Old Dominion University

Follow this and additional works at: https://digitalcommons.odu.edu/bioelectrics_pubs

 Part of the [Biochemistry Commons](#), [Biomedical Commons](#), [Biophysics Commons](#), and the [Molecular Biology Commons](#)

Repository Citation

Muratori, Claudia; Pakhomov, Andrei G.; Gianulis, Elena; Meads, Jade; Casciola, Maura; Mollica, Peter A.; and Pakhomova, Olga N., "Activation of the Phospholipid Scramblase TMEM16F by Nanosecond Pulsed Electric Field (nsPEF) Facilitates Its Diverse Cytophysiological Effects" (2017). *Bioelectrics Publications*. 196.

https://digitalcommons.odu.edu/bioelectrics_pubs/196

Original Publication Citation

Muratori, C., Pakhomov, A. G., Gianulis, E., Meads, J., Casciola, M., Mollica, P. A., & Pakhomova, O. N. (2017). Activation of the phospholipid scramblase TMEM16F by nanosecond pulsed electric field (nsPEF) facilitates its diverse cytophysiological effects. *Journal of Biological Chemistry*, 292(47), 19381-19391. doi:10.1074/jbc.M117.803049

Authors

Claudia Muratori, Andrei G. Pakhomov, Elena Gianulis, Jade Meads, Maura Casciola, Peter A. Mollica, and Olga N. Pakhomova



Activation of the phospholipid scramblase TMEM16F by nanosecond pulsed electric fields (nsPEF) facilitates its diverse cytophysiological effects

Received for publication, June 19, 2017, and in revised form, September 20, 2017. Published, Papers in Press, October 5, 2017, DOI 10.1074/jbc.M117.803049

Claudia Muratori^{‡1}, Andrei G. Pakhomov[‡], Elena Gianulis[‡], Jade Meads[‡], Maura Casciola[‡], Peter A. Mollica[§], and Olga N. Pakhomova[‡]

From the [‡]Frank Reidy Research Center for Bioelectrics, and the [§]Department of Medical Diagnostics and Translational Sciences, Old Dominion University, Norfolk, Virginia 23508

Edited by Dennis R. Voelker

Nanosecond pulsed electric fields (nsPEF) are emerging as a novel modality for cell stimulation and tissue ablation. However, the downstream protein effectors responsible for nsPEF bioeffects remain to be established. Here we demonstrate that nsPEF activate TMEM16F (or Anoctamin 6), a protein functioning as a Ca^{2+} -dependent phospholipid scramblase and Ca^{2+} -activated chloride channel. Using confocal microscopy and patch clamp recordings, we investigated the relevance of TMEM16F activation for several bioeffects triggered by nsPEF, including phosphatidylserine (PS) externalization, nanopore-conducted currents, membrane blebbing, and cell death. In HEK 293 cells treated with a single 300-ns pulse of 25.5 kV/cm, *Tmem16f* expression knockdown and TMEM16F-specific inhibition decreased nsPEF-induced PS exposure by 49 and 42%, respectively. Moreover, the *Tmem16f* silencing significantly decreased Ca^{2+} -dependent chloride channel currents activated in response to the nanoporation. *Tmem16f* expression also affected nsPEF-induced cell blebbing, with only 20% of the silenced cells developing blebs compared with 53% of the control cells. This inhibition of cellular blebbing correlated with a 25% decrease in cytosolic free Ca^{2+} transient at 30 s after nanoporation. Finally, in TMEM16F-overexpressing cells, a train of 120 pulses (300 ns, 20 Hz, 6 kV/cm) decreased cell survival to 34% compared with 51% in control cells (*, $p < 0.01$). Taken together, these results indicate that TMEM16F activation by nanoporation mediates and enhances the diverse cellular effects of nsPEF.

Permeabilization of biological membranes by high voltage pulsed electric fields (PEF),² known as electroporation, is a versatile technique in biomedicine used for intracellular delivery of drugs, plasmid DNA, and siRNA, as well as for tissue and tumor ablation (1). More recently, the pulse duration has been shortened into the nanosecond range. The effects of such short

pulses have been shown to reach into the cell interior (2, 3), thereby giving rise to specific biological effects and opening of new opportunities to control cell function.

The best known primary effect of nanosecond pulsed electric fields (nsPEF) is the permeabilization of membranes including the plasma membrane, endoplasmic reticulum, and mitochondria (2–6). nsPEF triggers the formation of pores of nanometer size (nanopores) on the cell membrane (7–9). Nanopores lifetime are in the order of seconds or minutes (7, 8, 10). We previously reported that nanopores are not “plain holes” in the plasma membrane such as larger pores generated by longer pulses. They have peculiar conductive properties analogous to ion channels, such as voltage sensitivity, current rectification, and ion selectivity (8, 11, 12). The inward rectification, which is regarded by some authors as a hallmark of nanopore formation (12), is manifested by a non-linear enhancement of the inward current at the most negative membrane potentials in nsPEF-treated cells. Nanopores display preferential permeability to cations (8, 11, 12), which is consistent with expectations that they are lined up with negatively charged hydrophilic phosphate groups of the membrane phospholipids (13).

Nanoporation initiates a plethora of downstream physiological changes including rapid phosphatidylserine (PS) externalization (13, 14), cytoskeleton disassembly (15–18), cell swelling and blebbing (19–21), modulation of endogenous ion channels (22, 23), and necrosis and apoptosis (24–26). The diversity of these effects suggests that plasma membrane nanoporation may be the initial step in a complex chain of signaling cascades leading to deregulation of multiple physiological functions. Indeed, nanopore opening causes an immediate rise in the intracellular free Ca^{2+} concentration. Ca^{2+} is a versatile signal that triggers processes as diverse as cell motility, gene transcription, muscle contraction, and membrane trafficking (27). Cells may interpret nsPEF-induced Ca^{2+} transients as authentic Ca^{2+} signals and amplify them by the Ca^{2+} -induced Ca^{2+} -release process (3, 4, 6, 28, 29).

Among proteins directly modulated by Ca^{2+} , the TMEM16 family of membrane proteins, also known as anoctamins, plays key roles in a variety of physiological functions that range from ion transport, to phospholipid scrambling and to regulating other ion channels (30–32). In particular, TMEM16F, or Anoctamin 6 (ANO6), was found to be an essential effector for the Ca^{2+} -dependent exposure of PS on the cell surface (33).

This work was supported by a 2015 Air Force Office of Scientific Research MURI grant (to A. G. P.) on Nanoelectropulse-induced Electromechanical Signaling and Control of Biological Systems, administered through Old Dominion University. The authors declare that they have no conflicts of interest with the contents of this article.

¹ To whom correspondence should be addressed: 4211 Monarch Way, Norfolk, VA 23508. Tel.: 757-683-7044; Fax: 757-451-1010; E-mail: cmurator@odu.edu.

² The abbreviations used are: PEF, pulsed electric field(s); nsPEF, nanosecond pulsed electric field(s); PS, phosphatidylserine; CaCCinh-AO-1, Ca^{2+} -activated chloride channel inhibitor-AO1; BAPTA, 1,2-bis(2-aminophenoxy) ethane-*N,N,N',N'*-tetraacetic acid; DIC, differential interference contrast; BisTris, 2-[bis(2-hydroxyethyl)amino]-2-(hydroxymethyl)propane-1,3-diol.

Nanosecond pulsed electric fields activate TMEM16F

Suzuki and colleagues (33) reported that knockdown of *Tmem16f* in the Ba/F₃ cells decreases the rate of PS externalization induced by the Ca²⁺ ionophore, whereas TMEM16F overexpression strongly enhances PS exposure. Sequencing of chromosomal DNA also demonstrates that Scott's syndrome patients carry loss-of-function mutations in the gene encoding TMEM16F (33, 34). Scott's syndrome is a congenital bleeding disorder caused by the loss of Ca²⁺-dependent PS exposure (29). This syndrome is accompanied by other cellular defects such as impaired bleb formation in platelets and absence of microvesicles shedding in both platelets and erythrocytes (35, 36).

Following the discovery that TMEM16F is a Ca²⁺-dependent scramblase defective in patients with Scott's syndrome, Yang *et al.* (37) proposed that the increase in Ca²⁺ required to induce PS externalization depends on the Ca²⁺-permeable non-selective cation channel activity of TMEM16F itself. The properties of ion channels associated with TMEM16F are a matter of debate. In addition to a non-selective cation channel activity, TMEM16F has been reported to function as a swelling-activated Cl⁻ (38), outwardly rectifying Cl⁻ (39), and Ca²⁺-activated Cl⁻ channel (40–43). These results have been obtained under different experimental conditions, which may explain some of these differences. Overall the data support the idea that TMEM16F has a non-selective pore or, as proposed by Whitlock and Hartzell (44), the existence of multiple open conformations with different ion permeability.

There is also controversy regarding the link between ion channel and scramblase activity of TMEM16F. It is not known if anions, cations, and phospholipids move through one pore, different pores formed by TMEM16F dimers, or whether additional accessory proteins are required. Whitlock and Hartzell (44) recently proposed that TMEM16F-mediated PS externalization is associated with leakage of ions through the lipid scrambling pathway between the protein and the scrambling lipid head groups.

TMEM16F activation has also been associated with programmed cell death. Several studies reported that TMEM16F is activated during apoptosis (39, 40, 45). Martins and colleagues (39) found that cell death induced by staurosporine in Jurkat cells was reduced in *Tmem16f*-silenced cells. They also showed that TMEM16F facilitates apoptotic cell shrinkage (39).

Because TMEM16F functions closely mirror nsPEF-induced bioeffects, in the present study we asked whether TMEM16F is a downstream effector of nanoporation. Using confocal microscopy and whole-cell patch clamp we show that TMEM16F expression affects PS externalization, cell blebbing, calcium influx, nanopore currents, and cell death induced by nsPEF. These results demonstrate that TMEM16F is activated in response to nsPEF, and that TMEM16F activation facilitates diverse cellular effects downstream from nanoporation.

Results

TMEM16F activation contributes to nsPEF-induced phosphatidylserine externalization

Fig. 1A shows that a single 300-ns pulse (25.5 kV/cm) causes a sustained externalization of PS on the plasma membrane of HEK

293 cells. Similarly to what has been already reported (46), we found that PS appears more at the anode-facing pole of the cell and within minutes distributes uniformly on the cell membrane. Externalization of PS can occur through the activation of scramblases, which are Ca²⁺-dependent. Therefore, to gain insight into the mechanism involved in PS exposure after nsPEF, we studied its dependence on extracellular Ca²⁺. HEK 293 cells were treated with nsPEF in bath solutions containing either 2 or 0 mM Ca²⁺ and PS externalization was measured over time using the calcium-independent binding with FITC-tagged Lactadherin. Fig. 1B shows that in the absence of Ca²⁺, one 300-ns pulse (25.5 kV/cm) did not trigger PS externalization pointing at the involvement of a Ca²⁺-dependent scramblase activity. The identification of TMEM16F as an essential component for the Ca²⁺-dependent exposure of PS on the cell surface (33) prompted us to investigate whether this scramblase is relevant for nsPEF-induced PS externalization. To block TMEM16F scramblase activity we used the Ca²⁺-activated chloride channel inhibitor-AO1 (CaCCinh-AO-1). This inhibitor was reported to block both the Ca²⁺-dependent Cl⁻ channel and scramblase activities (47). HEK 293 cells were pre-treated with 25 μM CaCCinh-AO-1 for 5 min in the presence of Cy5-labeled Annexin V. In control samples, cells were preincubated with the same dilution of the inhibitor vehicle DMSO. After this incubation time, a single 300-ns pulse (25.5 kV/cm) was delivered to a small group of cells and the PS exposure on the cell surface was monitored by confocal microscopy. At 8 min post-nsPEF, blocking TMEM16F decreased nsPEF-induced PS exposure by 42% as compared with control samples (Fig. 1C).

To further prove the involvement of TMEM16F in nsPEF-induced PS externalization, the expression of the endogenous *Tmem16f* in HEK 293 was knocked down by specific siRNA. As shown in Fig. 1D, transfecting two different *Tmem16f* siRNA (siRNA *Tmem16f*-I and -II) decreased the expression level of the messenger RNA (mRNA) to 26 and 11% of that in the siRNA control cells, respectively. The rate of nsPEF-induced PS exposure was decreased in both siRNA *Tmem16f* transformants (Fig. 1E). At 5.5 min after treatment, PS externalization in siRNA *Tmem16f*-I and -II cells was reduced by 33 and 49%, respectively. Notably, the impairment in the scramblase activity efficiency correlated with the level of *Tmem16f* silencing.

To summarize, we found that nsPEF-induced PS externalization is dependent on extracellular Ca²⁺, and that both chemical and expression block of TMEM16F reduced PS exposure. Our results suggest that Ca²⁺ coming through nanopores activates TMEM16F.

Tmem16f knockdown affects both nsPEF-induced membrane blebbing and rise in cytosolic free Ca²⁺

In addition to the PS externalization, nsPEF initiates rapid membrane blebbing (20, 21). Morphologically these blebs resemble pseudopods and exhibit a fast directional growth toward the anode (20, 21). Fig. 2A shows that nsPEF induced pseudopod-like blebs in cells transfected with the control siRNA, whereas knockdown of *Tmem16f* gene expression significantly impaired this response. After nanoporation, only 20% of silenced cells developed blebs compared with 53% of the control ones (Fig. 2B, left graph). Moreover, among the actively blebbing cells, *Tmem16f* expression affected the development

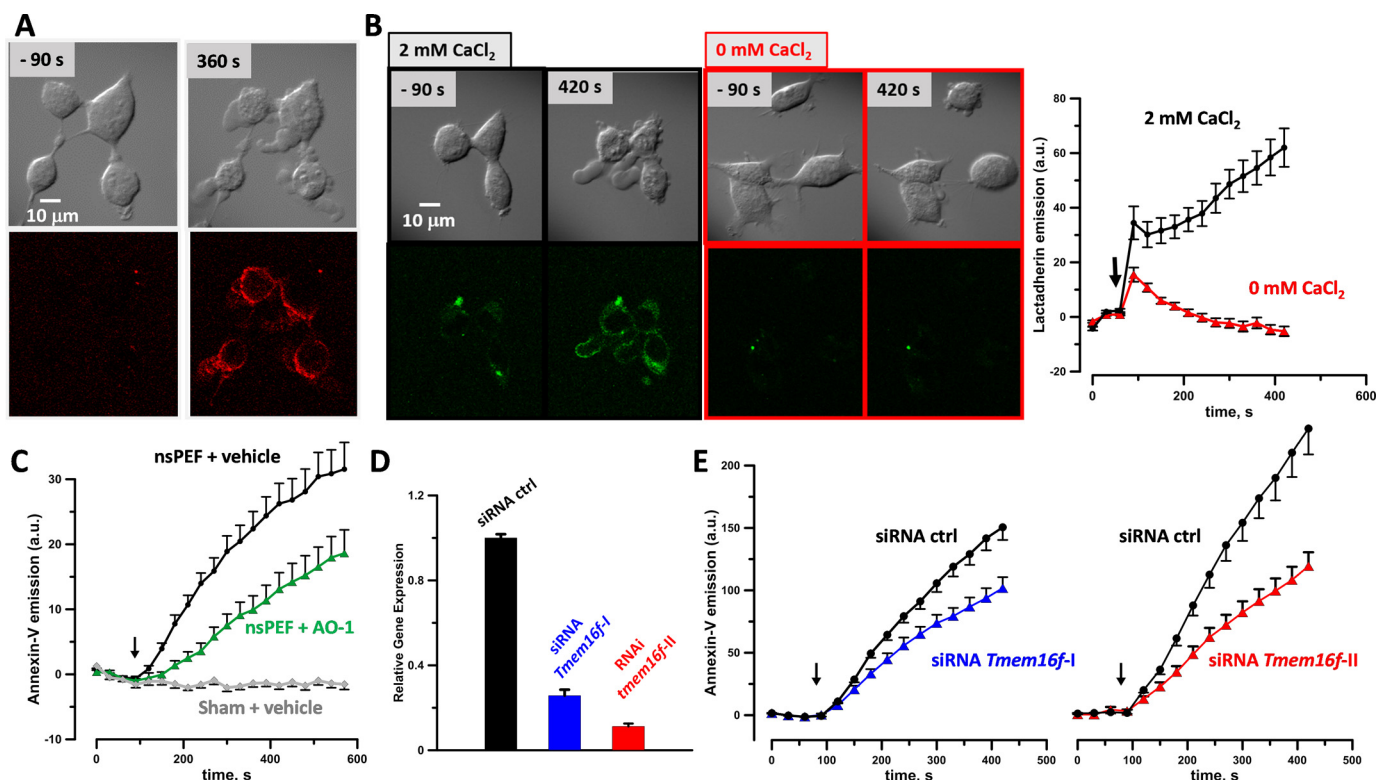


Figure 1. nsPEF-induced phosphatidylserine externalization (A), its dependence on Ca^{2+} (B), and on TMEM16F activity (C–E). HEK 293 were treated with a single 300-ns 25.5 kV/cm pulse, and PS externalization was monitored by time lapse confocal microscopy using either Cy5-labeled Annexin V (A, C, and E) or lactadherin-FITC (B). The nsPEF treatments were done at 87 s into the experiment (black arrows), after acquiring 3 pre-exposure images as a baseline. Panel A shows for a group of cells treated with nsPEF, DIC and Annexin V fluorescence images taken at the indicated time points. Panel B shows the lack of PS externalization in the absence of extracellular Ca^{2+} . Cells were treated with nsPEF in either 2 or 0 mM $CaCl_2$ bath solutions. DIC and lactadherin-FITC fluorescence images were taken at the indicated time points. In panel C, the scramblase activity of TMEM16F was blocked by incubation of cells with 25 μ M CaCCinh-AO-1 for 5 min. In control samples, the inhibitor vehicle DMSO was diluted the same way. Sham-exposed cells were not exposed to nsPEF but subjected to all the same manipulations. In panel D cells were transfected with two siRNA targeting *Tmem16f* transcripts (siRNA *Tmem16f*-I and -II) or scrambled siRNA and specific silencing was verified by real-time quantitative PCR. *Tmem16f* mRNA levels were normalized to *b-act* mRNA and are shown as relative expression. Panel E shows that silencing *Tmem16f* with two different siRNA sequences, *Tmem16f*-I (left) and -II (right), reduced the Annexin V emission curve in response to nsPEF. Mean \pm S.E., 35–46 (B), 35–40 (D), and 25–35 (E) cells per each group from 3 to 5 independent experiments.

of the blebs with the average bleb length for silenced cells decreased to $9.1 \pm 0.9 \mu$ m compared with $12.9 \pm 0.8 \mu$ m in control cells ($p < 0.01$, Fig. 2B, right graph). Notably, membrane blebbing in response to P2X purinergic receptor 7 (P2X₇R) activation was found to be dependent on *Tmem16f* expression (48) and cell bleb formation is compromised in platelets from Scott's syndrome patients (35, 36).

A downstream effect of nanoporation by nsPEF is the transient mobilization of calcium ions that involves both Ca^{2+} uptake from the outside and release from the endoplasmic reticulum (3, 4, 49, 50). A rise in cytosolic free calcium [Ca^{2+}]_i has been shown to have a pivotal role in bleb formation (51–53). We therefore asked whether the defects in membrane blebbing seen in *Tmem16f*-silenced cells correlated with an impairment in nsPEF-induced rise of [Ca^{2+}]_i. In the presence of 2 mM external Ca^{2+} , HEK 293 cells responded to one 300-ns pulse, 25.5 kV/cm with an immediate rise in [Ca^{2+}]_i (Fig. 2C), which lasted for minutes after the treatment. In silenced cells, the shape of the transients was similar to the control cell ones but reduced by 25%.

These results show that TMEM16F serves as a Ca^{2+} -permeable channel in nsPEF-treated cells. Both calcium influx and cell blebbing, two characteristic immediate responses to nsPEF, are reduced in *Tmem16f*-silenced cells.

Interplay between nanopore- and TMEM16F-conducted currents

Next, we explored if nsPEF increases Cl^- permeability of the cell membrane, and whether it is mediated by Ca^{2+} -mediated TMEM16F activation. In Fig. 3A, the whole-cell configuration was established 2 min prior the delivery of one 300-ns pulse at 4.2 kV/cm. The current-voltage (I-V) dependence was measured by applying the same voltage step protocol (–100 to +80 mV) at 30 s prior to nsPEF and again at 60 s after it. nsPEF increased the membrane conductance at both positive and negative potentials (Fig. 3A, left I-V curve). Substitution of the bath NaCl with sodium gluconate reduced the Cl^- concentration from 152.4 to 12.4 mM, thereby attenuating currents at the most positive membrane potentials with little or no impact on inward currents at negative potentials (Fig. 3A, right I-V curve). This result shows that nsPEF induces Cl^- currents. In principle these currents can flow through both nanopores and endogenous ion channels (including Ca^{2+} -dependent TMEM16F channel), although our previous studies showed that nanopores are cation-selective, with about 10-fold higher conductivity to K^+ than to Cl^- (12). To separate between Ca^{2+} -activated Cl^- current (presumably through TMEM16F) and other pathways of Cl^- influx, we varied the Ca^{2+} chelator load into the pipette.

Nanosecond pulsed electric fields activate TMEM16F

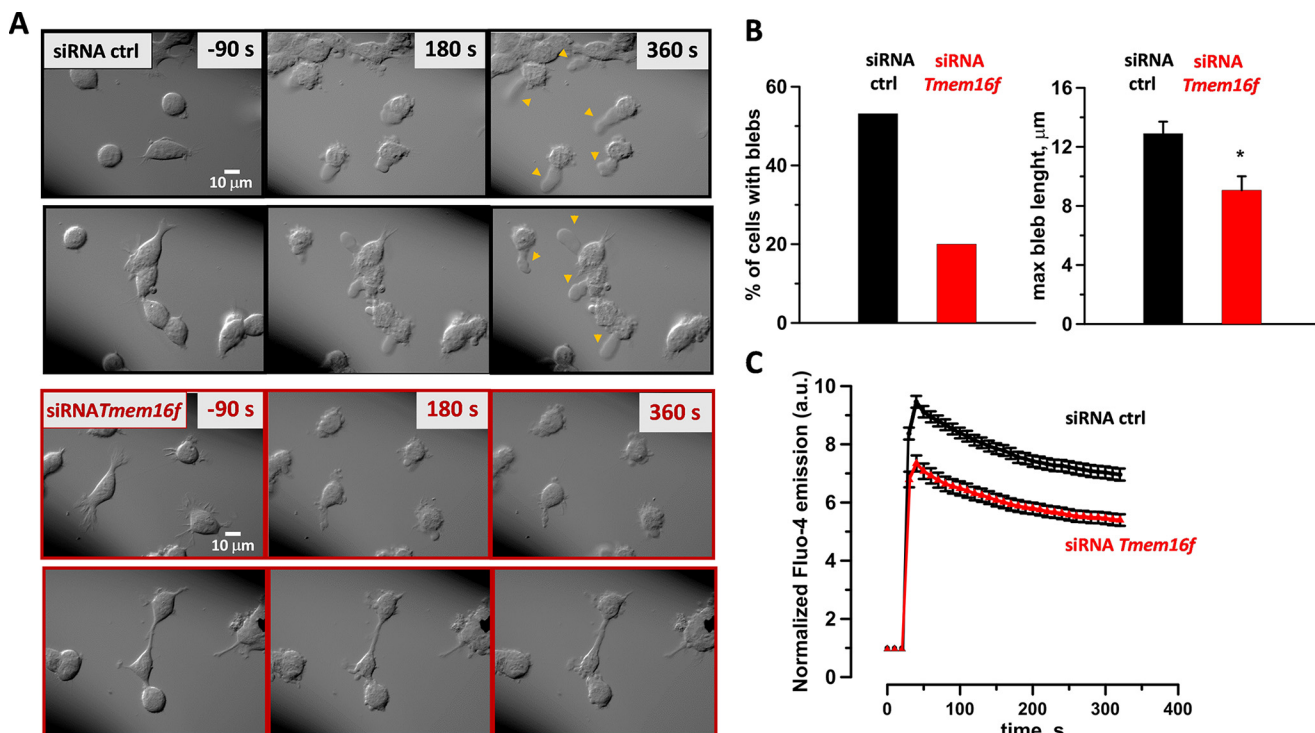


Figure 2. Silencing *Tmem16f* expression inhibits membrane blebbing (A and B) and reduced calcium transient (C) induced by nsPEF. HEK 293 cells silenced for *Tmem16f* expression were treated with one 300-ns 25.5 kV/cm pulse in the presence of 2 mM extracellular Ca^{2+} . Panel A shows the DIC images taken at the indicated time points of two representative groups of control (black) and *Tmem16f*-silenced (red) cells. At 360 s post-nsPEF, the yellow arrows indicate the pseudopod-like blebs. Quantification of the effects seen in A is shown in B. Blebs were measured at 360 s after nsPEF. Cells were considered bleb-positive when the length of the bleb exceeded the cell radius. In cells considered positive for blebbing, the maximum bleb length was calculated by measuring the longest bleb in each cell. Mean \pm S.E., 100–120 cells per each group from 3 independent experiments. *, $p < 0.01$. Panel C compares Ca^{2+} transients evoked by nsPEF in cells silenced for *Tmem16f* expression and control cells. The nsPEF treatment was done at 27 s into the experiment, after acquiring 3 pre-exposure images as a baseline, changes in cytosolic free calcium concentration were measured using Fluo-4. Each trace is the average from 50 cells.

With 2 mM extracellular Ca^{2+} , the cell cytoplasm was dialyzed using pipette solutions containing either 0.5 or 5 mM EGTA, or 5 mM BAPTA. At 30 s after one 300-ns pulse at 4.2 kV/cm, the I-V curves from cells dialyzed with the three solutions were very similar (Fig. 3B), suggesting that nanoporation was not affected by the availability of cytosolic free Ca^{2+} . This situation, however, changed over time: at 150 s after nsPEF, the current at the most positive membrane potentials in 0.5 mM EGTA cells was similar to the one at 30 s, whereas in 5 mM EGTA cells was significantly reduced. This difference became even more pronounced when using BAPTA which, compared with EGTA, has much faster Ca^{2+} -binding kinetics (54). In the subsequent experiments, we proved that this Cl^- current was indeed dependent on *Tmem16f* expression (Fig. 4). Using a pipette solution containing 0.5 mM EGTA, at 30 s after treatment with a single 300-ns pulse we recorded in both control and *Tmem16f*-silenced cells similar I-V curves. However, at 270 s after nsPEF, whereas the inward currents were still very similar, the outwardly ionic current of silenced cells was significantly reduced compared with control cells. These results show that the TMEM16F-mediated Cl^- conductance is activated by nsPEF in a Ca^{2+} -dependent manner with a few minutes delay after nsPEF exposure.

TMEM16F overexpression increases nsPEF cytotoxicity

The cytotoxicity of nsPEF have been demonstrated in multiple cell types *in vitro* (24, 25, 55–58). Because TMEM16F acti-

vation by nsPEF exacerbates cellular responses that have been linked to cell death such as PS externalization and cell blebbing (59), we anticipated that TMEM16F overexpression would increase nsPEF cytotoxicity. First we studied the sensitivity to nsPEF of HEK 293 exposed in suspension in electroporation cuvettes. Fig. 5A shows the effect of the increasing pulse number on cell survival, whereas other treatment parameters were fixed (20 Hz, 300-ns pulse duration, 6 kV/cm). A train of 120 pulses, which caused a 45% decrease of viability, was chosen to study the effect of TMEM16F overexpression on cell survival after nsPEF. Cells were exposed to nsPEF 48 h after transfection with either TMEM16F or a control construct. TMEM16F overexpression dropped cell survival to 34% compared with 51% in control samples (Fig. 5C). Considering that, on average, only about 50% of cells overexpressed the construct (Fig. 5B), the survival in the overexpressing cell subpopulation was estimated to be at ~17%.

Discussion

In the present study we show that TMEM16F, a protein that functions as a Ca^{2+} -dependent phospholipid scramblase and Ca^{2+} -activated Cl^- channel, is a downstream effector of nsPEF.

In light of our results, a key question is how nsPEF activates TMEM16F. Nanopores can remain open for minutes before being resealed (7, 8, 10), thus leading to rapid influx of Ca^{2+} , ionic imbalance, and cell swelling (24, 60). Notably, both intracellular Ca^{2+} elevation and cell swelling have been linked to

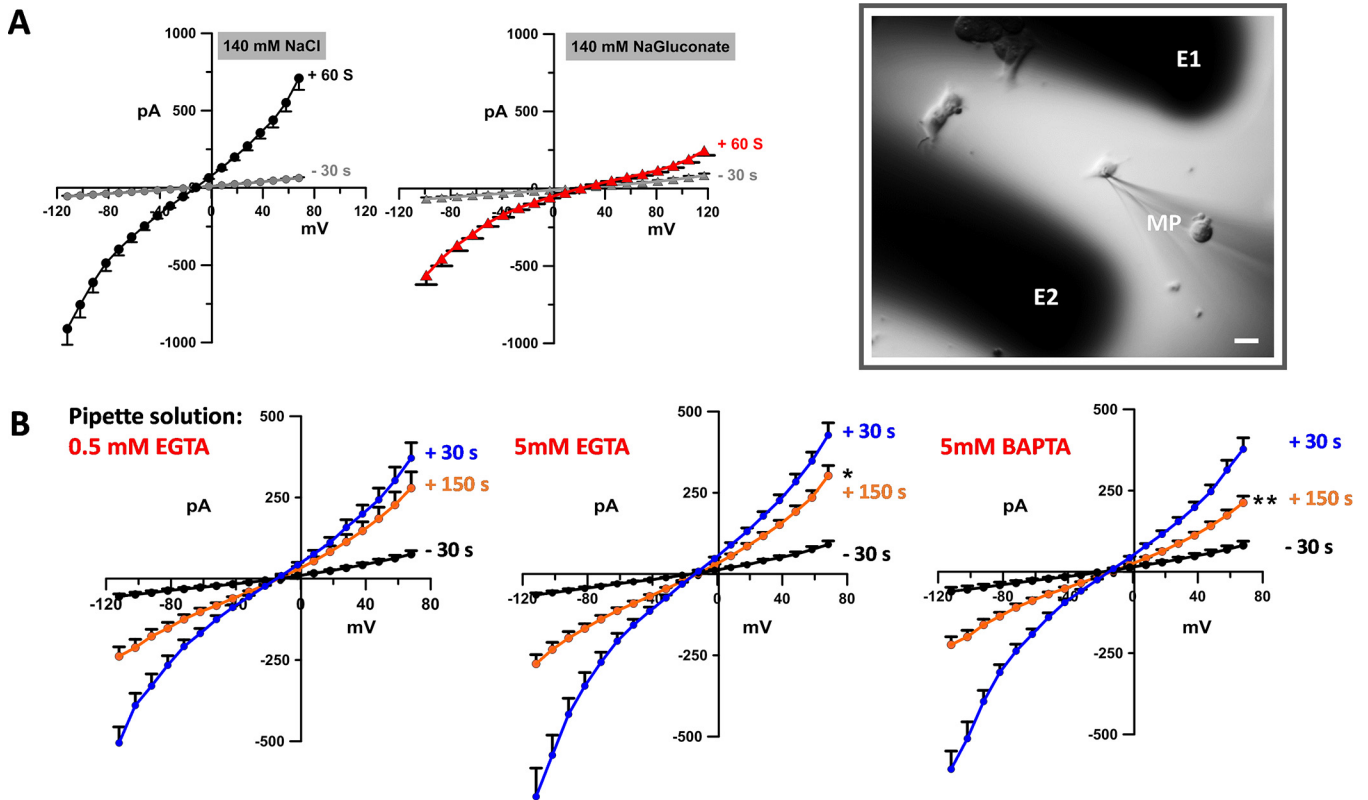


Figure 3. Nanopore current dependence on extracellular Cl^- (A) and intracellular free Ca^{2+} (B). HEK 293 cells were bathed with 2 mM extracellular CaCl_2 and, 2 min after the establishment of the whole cell configuration, subjected to one 300-ns pulse at 4.2 kV/cm. Panel A shows the effect on Cl^- replaced by Gluconate $^-$ on membrane currents in nsPEF-exposed cells. Currents were measured at 30 s prior to nsPEF and then after at 60 s. Mean \pm S.E., 15 cells per each group from 2 independent experiments. Inset shows the position of the PEF-delivering electrodes relative to the exposed cell and the recording pipette. Calibration bar: 20 μm . In panel B, the cytoplasm of the patched cells was dialyzed using pipette solutions containing either 0.5 or 5 mM EGTA, or 5 mM BAPTA. Currents were measured at the indicated time points relative to the moment of nsPEF delivery. Mean \pm S.E., 10 cells per each group from 3 independent experiments. *, $p < 0.05$; **, $p < 0.001$ for the difference between +30 and +150 s.

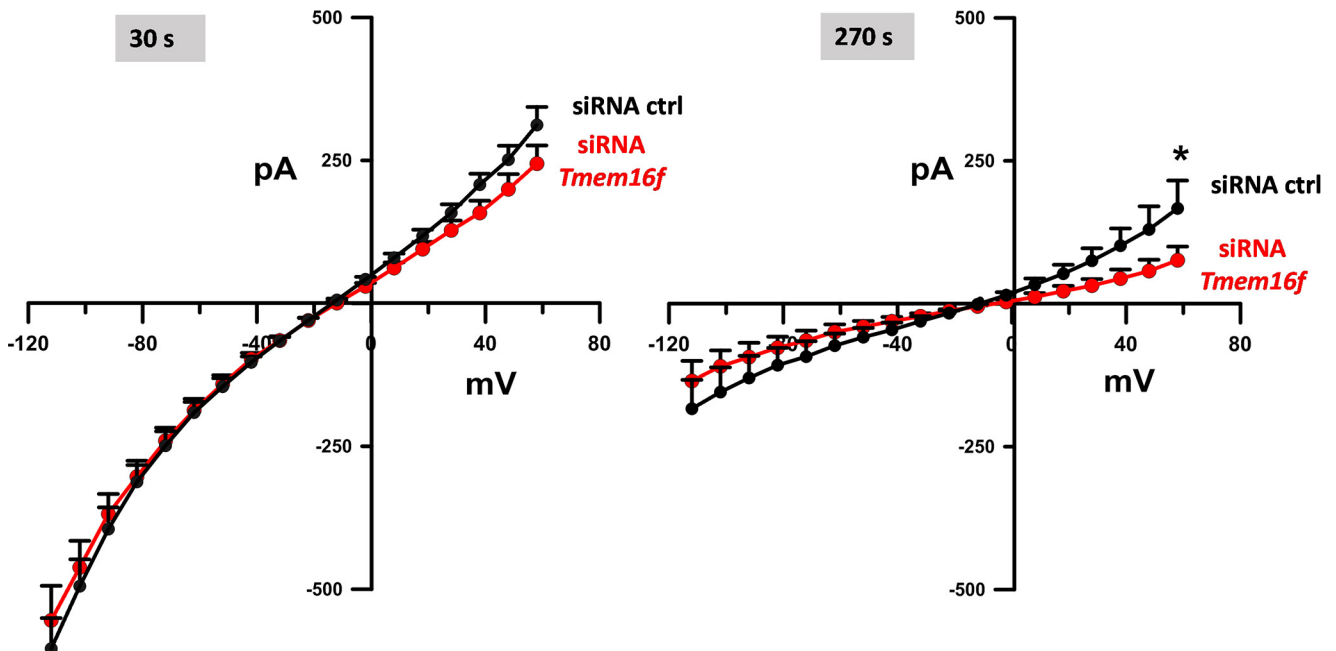


Figure 4. Silencing *Tmem16f* expression suppresses currents at positive membrane potentials. I-V curves for control and *Tmem16f*-silenced cells measured at 30 and 270 s after nsPEF (one 300-ns, 4.2 kV/cm). Values were corrected for their parallel sham exposure measurements. Mean \pm S.E., 14–16 cells per each group from 4 independent experiments. *, $p < 0.05$ for the difference between control and *Tmem16f*-silenced samples.

Nanosecond pulsed electric fields activate TMEM16F

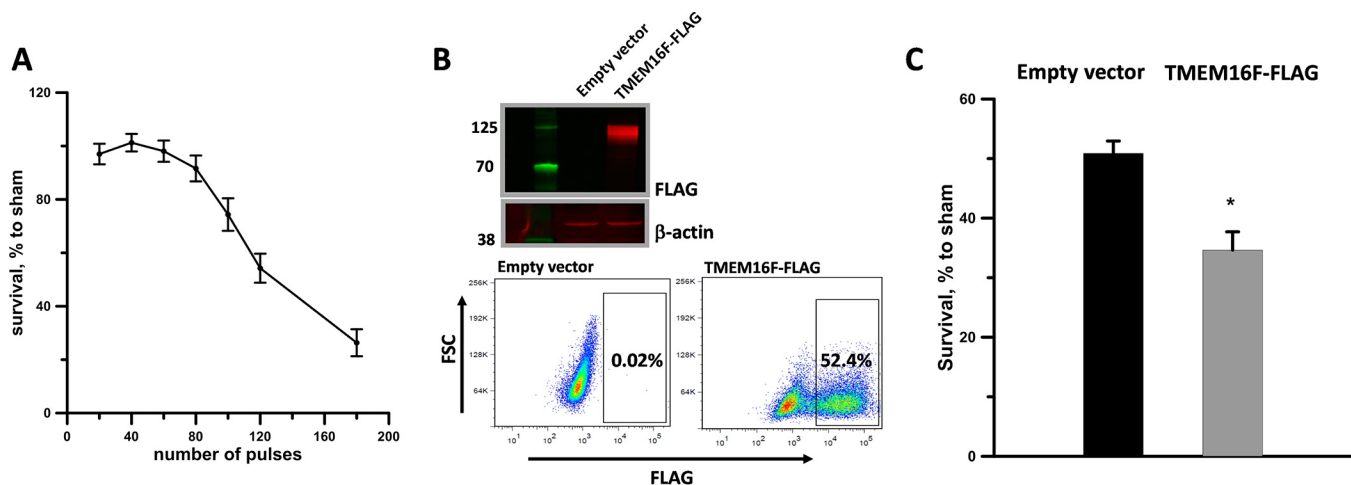


Figure 5. The effect of pulse number (A) and TMEM16F overexpression on HEK 293 cell death (B and C). A, cells were treated with increasing numbers of 300-ns pulses (20 Hz at 6 kV/cm). Exposures were performed in 1-mm gap electroporation cuvettes and cell survival was assessed in 24 h. Results are expressed in % to sham-exposed parallel control at 24 h. Mean \pm S.E. for 9 independent experiments. B, expression level of TMEM16F-3xFLAG analyzed by Western blot and FACS analyses at 48 h after transfection. Extracts of cells were immunoblotted with an anti-FLAG and, as a control, with β -actin antibody. TMEM16F is seen as a broad band around 120 kDa. To measure the % of TMEM16F-positive cells, control and overexpressing cells were permeabilized, stained with an anti-FLAG antibody, and analyzed by FACS. Cells in the gated area were considered positive for TMEM16F expression. C, overexpression of TMEM16F increases the cytotoxicity of exposure to 120 pulses (300-ns width, 6 kV/cm, 20 Hz). The survival was measured at 24 h after nsPEF exposure and expressed in % to sham-exposed parallel control. Mean \pm S.E. for 6 independent experiments. *, $p < 0.001$.

TMEM16F activation. Ionomycin, P2Y₂ receptors activation, and direct elevation of cytosolic Ca²⁺ using specific patch pipette solutions as well as hypotonic bath solutions all activate TMEM16F-dependent Cl⁻ currents (38, 40, 41, 48, 61). Our results show that Ca²⁺ coming through nanopores is sufficient to activate TMEM16F. We found that depletion of the extracellular Ca²⁺ completely abolished PS exposure in nanoporated cells and that the cytosolic chelation of Ca²⁺ coming through nanopores reduced TMEM16F-mediated Cl⁻ conductance. The relevance of the osmotic cell swelling for TMEM16F channel activation in nanoporated cells has yet to be explored.

Permeabilization of the cell membrane by nsPEF causes rapid PS externalization (13, 14). Results from both experiments and molecular dynamics simulations support the idea that nsPEF-induced PS translocation is a result of an electrophoretic migration of the negatively charged PS head group alongside the lipid-water interface of nanopores (62–64). Our results point, for the first time, to the involvement of activated scramblase in nsPEF-induced PS externalization. Both chemical inactivation of TMEM16F and gene silencing significantly reduced nsPEF-induced PS exposure. We also show that PS externalization is abolished when cells are treated with nsPEF in the absence of extracellular Ca²⁺. These results suggest that PS exposure in nanoporated cells happens exclusively in a scramblase-dependent manner. However, Ca²⁺ affects the plasma membrane electroporation itself. We previously reported that pore formation and evolution are dependent on external Ca²⁺ (65). In particular, we found that Ca²⁺ first stabilizes the pores but facilitates their delayed expansion (65). Therefore one should consider that, in addition to activating TMEM16F, in nanoporated cells Ca²⁺ may affect PS exposure by modulating the structure and stability of the pores. Indeed, direct blockage of TMEM16F did not abolish PS externalization suggesting that both scramblase activation and lateral drift throughout nanopores may drive nsPEF-induced phospholipid perturbation. The balance between these two mechanisms may

depend on the pulse parameters and on whether the influx of Ca²⁺ through the nanopores is sufficient to stimulate scramblase activity.

We also found that TMEM16F gene silencing markedly reduced cell blebbing occurring in response to nsPEF. Blebs are a result of actomyosin contraction, which causes transient detachment of the cell membrane from the actin cortex. Their expansion is rapid and dependent on actin polymerization (66). Cortical contractility is associated with cyclic intracellular calcium transients (67, 68). Although it has been reported that Scott's syndrome patients have cell blebbing and microvesicles shedding defects, the mechanisms by which TMEM16F controls these processes are unknown. One can speculate that the TMEM16F non-selective cation channel activity is responsible for the rise in cytosolic free Ca²⁺ crucial for bleb formation. Indeed, we found a 25% calcium transient reduction in *Tmem16f*-silenced cells. However, whether this difference is enough to explain the blebbing impairment seen in silenced cells, as well as the direct role of the TMEM16F cation channel activity needs to be further investigated.

To assess the activation of the TMEM16F channel, we focused on the Cl⁻ currents. Using both overexpression and silencing approaches, several groups showed that TMEM16F can conduct Cl⁻ currents in response to the elevation of the intracellular Ca²⁺ concentration (40–43, 69).

nsPEF caused a long-lasting increase of cell membrane conductance, both at positive and negative membrane potentials. Removal of the extracellular Cl⁻, chelating of the cytosolic Ca²⁺, and changing *Tmem16f* expression affected the current at the positive but not negative membrane potentials. Considering our earlier data that nanopore currents are maximized at negative membrane potentials (8, 11, 12), and that nanopores are strongly selective for cations (8, 11, 12), these new findings provide strong evidence that nsPEF activates TMEM16F function as a Cl⁻ channel. Moreover, this activation was observed minutes after the

mobilization of cytosolic Ca^{2+} , which is consistent with earlier reports that Ca^{2+} -dependent Cl^- current through TMEM16F channel takes minutes to develop (41, 43, 69).

TMEM16F is not the first ion channel found to respond to nsPEF. Indeed, several groups including ours reported activation of voltage-gated calcium channels in response to nsPEF as well as a long lasting inactivation of both voltage-gated calcium channels and voltage-gated sodium channels by an unknown mechanism (23, 29, 70–73).

Activation of ion channels is an important step for regulated cell death (74). Our data show that nsPEF cytotoxicity is increased when TMEM16F is overexpressed in nanoporated cells. Depending on the pulse parameters, exposure method, and cell type used, *in vitro* studies showed that nsPEF can activate apoptosis, necrosis, a combination of these mechanisms, and autophagy (24, 55, 75). Although it is not uncommon that a death stimulus activates more than one cell death pathway, it is not clear how nsPEF does it. Notably, TMEM16F was reported to be activated during both apoptosis and necroptosis, a programmed form of necrosis (39, 40, 45, 76). Activation of TMEM16F by a mild increase of intracellular Ca^{2+} induces Cl^- -selective currents, cell shrinkage, and apoptosis (39, 40, 45). At strong activation, e.g. by stimulation of purinergic P2Y₇ receptors, TMEM16F participates in pore formation, massive membrane blebbing, cell swelling, and necroptotic cell death (48). Based on these findings, one could expect that the mechanism and level of TMEM16F activation may influence the cell death mode in nsPEF-treated cells.

Taken together, we demonstrate that TMEM16F is an important regulator of the cellular effects of downstream nanoporation. Our results provide new insight into the mechanisms of action of nsPEF stimulation.

Experimental procedures

Cell culture, chemicals, and solutions

HEK 293 cells were kindly provided by Dr. John Catravas (Old Dominion University, Frank Reidy Research Center for Bioelectrics, Norfolk, VA). Cells were cultured in Eagle's minimum essential medium with L-glutamine (ATCC), supplemented with 10% (v/v) fetal bovine serum (certified OneShot format, FBS-OneShot, Life Technologies). One day prior to the experiments, cells were passaged and transferred onto glass coverslips (number 0 thickness, 10 mm diameter) pretreated with 20 ng/ml of Laminin (Sigma) to improve cell adhesion.

The composition of solutions utilized in different experiments is described below. Chemicals were purchased from Sigma and Life Technologies. The osmolality of the solutions was between 290 and 310 milliosmole/kg, as measured by a freezing point microosmometer (Advanced Instruments, Inc., Norwood, MA). All experiments were performed at room temperature ($22 \pm 2^\circ\text{C}$).

nsPEF exposure methods

nsPEF was delivered to cells either attached to glass coverslips or in suspension in electroporation cuvettes. Both methods have been previously described (8, 77). For cells on glass coverslips, nearly rectangular 300-ns pulses were generated by a Mosfet-switch-based circuit upon delivery of a TTL trigger pulse from pClamp software via a Digidata 1322A output

(Molecular Devices). The same software and Digidata output were used to synchronize nsPEF exposure, image acquisition, and whole-cell recordings. nsPEF were delivered to a selected cell or small group of cells with a pair of tungsten rod electrodes (100 μm diameter, 140 μm gap). The electrodes were positioned precisely 30 μm or, for the electrophysiology experiments, 40 μm above the coverslip using a robotic manipulator (MP-225, Sutter Instruments, Novato, CA). In most experiments we delivered one 300-ns pulse at 25.5 kV/cm; for electrophysiology experiments pulse intensity was reduced to 4.25 kV/cm. The E field at the cell location was calculated as described previously (78), by 3D numerical simulations using a finite element analysis software COMSOL Multiphysics®, release 5.0 (COMSOL Inc., Stockholm, Sweden).

For cells in suspension, trains of trapezoidal pulses of 300 ns duration (20 Hz, 6 kV/cm) from an AVTECH AVOZ-D2-B-ODA generator (AVTECH Electrosystems, Ottawa, Ontario, Canada) were delivered to 1-mm gap electroporation cuvettes (BioSmith, San Diego, CA) via a 50- to 10-ohm transition module (AVOZ-D2-T, AVTECH Electrosystems) modified into a cuvette holder. To produce pulse trains of predetermined duration at selected repetition rates, the generator was triggered externally from a model S8800 stimulator (Grass Instrument Co., Quincy, MA). The pulse amplitude and shape were monitored in all experiments using a 500 MHz, 5 GS/s TDS 3052B oscilloscope (Tektronix, Wilsonville, OR).

PS externalization and calcium imaging

To study both PS externalization and Ca^{2+} influx in response to nsPEF, a coverslip with cells was placed in a glass-bottomed chamber (Warner Instruments, Hamden, CT) mounted on an Olympus IX81 inverted microscope equipped with an FV 1000 confocal laser scanning system (Olympus America, Center Valley, PA). The chamber was filled with a physiological solution containing (in mM): 140 NaCl, 5.4 KCl, 1.5 MgCl_2 , 2 CaCl_2 , 5 HEPES, 10 glucose (pH 7.4 with NaOH).

To detect PS externalization we used either a Ca^{2+} -dependent Cy5-labeled Annexin V (BD Biosciences, San Jose, CA) or a Ca^{2+} -independent bovine lactadherin-FITC (Hematologic Technologies, Essex, VT). Cy5-labeled Annexin V was diluted 1:100 in the physiological solution. Lactadherin-FITC was used at 0.25 $\mu\text{g}/\text{ml}$ in physiological solutions containing either 2 mM CaCl_2 or 0 mM CaCl_2 and 2 mM EGTA. To block TMEM16F, we used CaCCinh-AO-1 from Sigma. The inhibitor was resuspended in 50 mM DMSO and diluted 1:2000 to a final concentration of 25 μM . In control samples DMSO was diluted the same way. Differential interference contrast (DIC) and fluorescent images were taken with a $\times 40$, NA 0.95 dry objective as a time series (1 image/30 s) beginning 87 s before nsPEF exposure and continuing for up to 8 min after. Cy5-labeled Annexin V was excited with a red laser (635 nm) and the emission of the dye was detected between 655 and 755 nm. Lactadherin-FITC was excited with a blue laser (488 nm) and the emission of the dye was detected between 505 and 605 nm.

The cytosolic Ca^{2+} was monitored by fluorescence imaging with Fluo-4 (Invitrogen). To load the cells with the dye, the coverslips were incubated for 15 min in the physiological solution containing 5 μM Fluo-4/AM and 0.02% of Pluronic F-127

Nanosecond pulsed electric fields activate TMEM16F

(Life Technologies), in the dark at room temperature. The coverslips were rinsed twice and then left for 15 min in the physiological solution before being transferred into the glass-bottomed chamber.

DIC and fluorescence images were taken as a time series (1 image/10 s) starting at 27 s before nsPEF treatment and continuing for 4.8 min. Fluo-4 was excited with a green laser (488 nm) and the emission of the dye was detected between 505 and 605 nm. Images were quantified using MetaMorph Advanced version 7.7.0.0 (Molecular Devices, Foster City, CA).

Electrophysiology

Whole-cell patch clamp recordings were conducted similarly to what was previously described (8, 10, 79). Recording pipettes were pulled from borosilicate glass (BF150-86-10, Sutter Instruments, Novato, CA) to a tip resistance of 1.5–3 M Ω using a Flaming/Brown P-97 puller (Sutter Instruments).

HEK 293 cells plated on coverslips were placed in the same microscope setup as was used for cell imaging. In most experiments the bath solution contained (in mM): 140 NaCl, 5.4 KCl, 1.5 MgCl₂, 2 CaCl₂, 5 HEPES, and 10 glucose. For experiments described in Fig. 3A, 140 mM NaCl was replaced with 140 mM sodium gluconate. The pipette solution contained (in mM): 140 cesium acetate, 4 MgCl₂, 10 HEPES and either 0.5 (Figs. 3B and 4) or 5 cesium-EGTA (Fig. 3, A and B), or 5 cesium-BAPTA (Fig. 3B). In the experiment described in Fig. 3B, we blocked the 2 mM Ca²⁺ coming through the nanopores by using pipette solutions with different Ca²⁺ buffering efficiency. We used a solution with low Ca²⁺ binding capacity, 0.5 mM EGTA (1.5 mM free Ca²⁺), and two solutions with comparable high Ca²⁺ binding capacity, 5 mM EGTA (60 mM free Ca²⁺) and 5 mM BAPTA (160 mM free Ca²⁺), but different binding kinetics. BAPTA, compared with EGTA, has much faster Ca²⁺-binding kinetics (54). The free calcium concentration was calculated with Ca/Mg, ATP/EGTA Calculator version 2.2b (web.stanford.edu/~cpatton/webmaxcS.htm).³ The pH of both bath and pipette solutions was adjusted to 7.4.

Two minutes after the whole-cell configuration was established, membrane currents were recorded at specific times before and after nsPEF exposure by applying the same voltage-step protocol (200 ms steps from –100 to 70 mV in 10-mV increments); the holding potential between the sweeps was set at –70 mV. Data were collected using a Multiclamp 700B amplifier, Digidata 1322A A–D converter, and pCLAMP 10 software (Molecular Devices). All voltage values reported in the graphs were corrected for respective junction potentials.

Tmem16f expression knockdown and overexpression

To silence *Tmem16f* expression, we used two different stealth siRNA: HSS153251 (siRNA *Tmem16f*-I) and HSS176378 (siRNA *Tmem16f*-II) (Invitrogen). To transfect the siRNA we used Lipofectamine RNAiMAX (Invitrogen) according to the manufacturer's instructions. Control samples were transfected with stealth siRNA negative control medium GC duplex (Invitrogen).

To overexpress TMEM16F, we used a mouse TMEM16F-3xFLAG (80) construct kindly provided by Dr. Criss Hartzell

(Emory University School of Medicine, Department of Cell Biology, Atlanta, GA). The construct was transfected in HEK 293 using Lipofectamine 2000 (Invitrogen) according to the manufacturer's instructions. Control samples were treated the same way and transfected with an empty control vector. Experiments with both silenced and overexpressing cells were done at 48 h post-transfection.

RT-PCR, Western blot, and FACS analyses

Total RNA was extracted from $\sim 5 \times 10^5$ cells using TRIzolTM (Invitrogen) following the manufacturer's protocol. RNA quantity and quality were assessed by absorbance at 260/280 nm using a NanoDrop 2000 (Thermo Fisher, Waltham, MA), with 260/280 ratios between 1.8 and 2.0. Residual genomic DNA was degraded from 1 μ g of total RNA using DNase I, Amplification Grade (Thermo Fisher). One μ g of each experimental sample was reverse transcribed into cDNA using a High Capacity cDNA Reverse Transcription Kit (Applied Biosystems, Foster City, CA) according to the suggested manufacturer's protocol. Gene expression analysis was conducted on samples using TaqMan Gene Expression Assays for *Tmem16f* (Hs03805835_m10.51), and the endogenous housekeeping gene *b-act* (Hs99999903_m1). Real-time quantitative PCR was conducted with a StepOnePlusTM Real-time PCR System (Applied Biosystems) using TaqManTM Fast Advanced Master Mix (Life Technologies) and 10 ng of cDNA for each sample. All experimental reactions were performed in triplicate. Negative controls were included for all reactions, with nuclease-free water substituted for cDNA samples. Each cDNA sample was subsampled 3 times during each quantitative PCR. Relative fold-changes were calculated using the $2^{-\Delta\Delta C_t}$ method. Significance was determined by comparing the $2^{-\Delta C_t}$ value using a one-way analysis of variance with a Dunnett's post hoc. Error bars represent the standard deviation of the relative-fold expression between samples.

The Western blot procedure was described previously (81). At 48 h after transfection, cells were lysed in a buffer containing 20 mM HEPES (pH 7.5), 200 mM NaCl, 10 mM EDTA, 1% Triton X-100, supplemented with the SIGMAFAST mixture of protease inhibitors (Sigma). Proteins in the lysate were separated by electrophoresis on a NuPAGE 4–12% BisTris SDS-polyacrylamide gel (Life Technologies) and then transferred to Immune-Blot Low Fluorescence PVDF membrane (Bio-Rad). The membranes were blocked in the Odyssey blocking buffer for 1 h at room temperature (LI-COR Biosciences, Lincoln, NE). The primary mouse anti-FLAG M2 monoclonal antibody (Sigma) was diluted to a final concentration of 1 μ g/ml in the Odyssey blocker with 0.2% Tween 20. The secondary goat anti-mouse IgG (H+L) antibody, conjugated with an infrared fluorophore IRDye-680LT (LI-COR Biosciences), was diluted 1:20,000 in the same buffer. The membranes were incubated at room temperature with primary and secondary antibodies for 2 and 1 h, respectively. The membranes were imaged using the Odyssey 9120 Infrared Imaging System (LI-COR Biosciences) in the 700-nm channel.

Quantification of the cells overexpressing TMEM16F was done by FACS analysis. At 48 h after transfection, 1×10^6 HEK 293 cells per sample were fixed and permeabilized using the Fix and Perm cell permeabilization reagent (Molecular Probes,

³ Please note that the JBC is not responsible for the long-term archiving and maintenance of this site or any other third party hosted site.

Eugen, OR) according to manufacturer's instructions. The primary anti-FLAG M2 (Sigma) and secondary Alexa Fluor 488 goat anti-mouse IgG (H+L) (Life Technologies) antibodies were diluted to a final concentration of 2 and 1 $\mu\text{g}/\text{ml}$, respectively, and incubated for 30 min at room temperature. Samples were acquired using a MACSQuant Analyzer 10 flow cytometer (Miltenyi Biotec, Bergisch Gladbach, Germany) and analyzed with FlowJo software (FlowJo, Ashland, OR).

Viability assay

At 48 h after transfection, cells were detached by treatment with 0.5 mg/ml of trypsin-EDTA, resuspended at 1.2×10^6 cell/ml in fresh medium, and 100- μl samples of this suspension were aliquoted to electroporation cuvettes for nsPEF exposures. Immediately following the exposures, the samples were diluted with fresh medium to 3×10^5 cells/ml and aliquoted into a 96-well plate, in triplicates at 30×10^3 cell/well and left at 37 °C in the incubator. At 24 h after the exposure, 10 μl of Presto Blue reagent (Life Technologies) was added to each well and the incubation continued for 1 h at 37 °C. The plate was read with a Synergy 2 microplate reader (BioTek, Winooski, VT), with excitation/emission settings at 530/590 nm. The triplicate data were averaged, corrected for the background, and considered as a single experiment.

Statistical analysis

Unless specified otherwise, data are presented as mean \pm S.E. for n independent experiments. Statistical analyses were performed using a two-tailed t test where $p < 0.05$ was considered statistically significant. Statistical calculations, including data fits, and data plotting were accomplished using Grapher 11 (Golden Software, Golden, CO).

Author contributions—C. M., O. N. P., and A. G. P. conceived and designed the study and wrote the manuscript. C. M. performed and analyzed the experiments shown in Figs. 1 and 2. C. M. and E. G. performed and analyzed the experiments shown in Figs. 2 and 3. J. M. and P. A. M. conducted the experiments and data analysis shown in Fig. 5. M. C. conducted the electric field simulations. All authors analyzed the results and approved the final version of the manuscript.

Acknowledgments—We thank Dr. Criss Hartzell and Dr. Yuan Yuan Cui (Emory University School of Medicine, Dept. of Cell Biology, Atlanta, GA), Dr. Donald Hilgemann and Dr. Michael Fine (Dept. of Physiology, the University of Texas Southwestern Medical Center, Dallas, TX), Dr. John Catravas and Dr. Yu Jing (Frank Reidy Research Center for Bioelectrics, Old Dominion University, Norfolk, VA), and Dr. Robert Bruno (Dept. of Medical Diagnostics and Translational Sciences, Old Dominion University, Norfolk, VA) for valuable discussions and help provided during the study.

References

1. Yarmush, M. L., Golberg, A., Serša, G., Kotnik, T., and Miklavcic, D. (2014) Electroporation-based technologies for medicine: principles, applications, and challenges. *Annu. Rev. Biomed. Eng.* **16**, 295–320
2. Schoenbach, K. S., Hargrave, B., Joshi, R. P., Kolb, J., Osgood, C., Nuccitelli, R., Pakhomov, A. G., Swanson, J., Stacey, M., White, J. A., Xiao, S., Zhang, J., Beebe, S. J., Blackmore, P. F., and Buescher, E. S. (2007) Bioelectric effects of nanosecond pulses. *IEEE Trans. Dielectrics Elec. Insul.* **14**, 1088–1109
3. Semenov, I., Xiao, S., and Pakhomov, A. G. (2013) Primary pathways of intracellular Ca^{2+} mobilization by nanosecond pulsed electric field. *Biochim. Biophys. Acta* **1828**, 981–989
4. Semenov, I., Xiao, S., Pakhomova, O. N., and Pakhomov, A. G. (2013) Recruitment of the intracellular Ca by ultrashort electric stimuli: the impact of pulse duration. *Cell Calcium* **54**, 145–150
5. Batista Napotnik, T., Wu, Y. H., Gundersen, M. A., Miklavcic, D., and Vernier, P. T. (2012) Nanosecond electric pulses cause mitochondrial membrane permeabilization in Jurkat cells. *Bioelectromagnetics* **33**, 257–264
6. White, J. A., Blackmore, P. F., Schoenbach, K. H., and Beebe, S. J. (2004) Stimulation of capacitative calcium entry in HL-60 cells by nanosecond pulsed electric fields. *J. Biol. Chem.* **279**, 22964–22972
7. Bowman, A. M., Nesin, O. M., Pakhomova, O. N., and Pakhomov, A. G. (2010) Analysis of plasma membrane integrity by fluorescent detection of Ti^{+} uptake. *J. Membr. Biol.* **236**, 15–26
8. Pakhomov, A. G., Bowman, A. M., Ibey, B. L., Andre, F. M., Pakhomova, O. N., and Schoenbach, K. H. (2009) Lipid nanopores can form a stable, ion channel-like conduction pathway in cell membrane. *Biochem. Biophys. Res. Commun.* **385**, 181–186
9. Gowrishankar, T. R., and Weaver, J. C. (2006) Electrical behavior and pore accumulation in a multicellular model for conventional and supra-electroporation. *Biochem. Biophys. Res. Commun.* **349**, 643–653
10. Pakhomov, A. G., Kolb, J. F., White, J. A., Joshi, R. P., Xiao, S., and Schoenbach, K. H. (2007) Long-lasting plasma membrane permeabilization in mammalian cells by nanosecond pulsed electric field (nsPEF). *Bioelectromagnetics* **28**, 655–663
11. Pakhomov, A. G., Shevin, R., White, J. A., Kolb, J. F., Pakhomova, O. N., Joshi, R. P., and Schoenbach, K. H. (2007) Membrane permeabilization and cell damage by ultrashort electric field shocks. *Arch. Biochem. Biophys.* **465**, 109–118
12. Pakhomov, A. G., and Pakhomova, O. N. (2010) Nanopores: A distinct transmembrane passageway in electroporated cells. in *Advanced Electroporation Techniques in Biology in Medicine* (Pakhomov, A. G., Miklavcic, D., and Markov, M. S., eds) pp. 178–194, CRC Press, Boca Raton, FL
13. Vernier, P. T., Sun, Y., Marcu, L., Craft, C. M., and Gundersen, M. A. (2004) Nanoelectropulse-induced phosphatidylserine translocation. *Bioophys. J.* **86**, 4040–4048
14. Vincelette, R. L., Roth, C. C., McConnell, M. P., Payne, J. A., Beier, H. T., and Ibey, B. L. (2013) Thresholds for phosphatidylserine externalization in Chinese hamster ovarian cells following exposure to nanosecond pulsed electrical fields (nsPEF). *PLoS ONE* **8**, e63122
15. Berghöfer, T., Eing, C., Flickinger, B., Hohenberger, P., Wegner, L. H., Frey, W., and Nick, P. (2009) Nanosecond electric pulses trigger actin responses in plant cells. *Biochem. Biophys. Res. Commun.* **387**, 590–595
16. Pakhomov, A. G., Xiao, S., Pakhomova, O. N., Semenov, I., Kuipers, M. A., and Ibey, B. L. (2014) Disassembly of actin structures by nanosecond pulsed electric field is a downstream effect of cell swelling. *Bioelectrochemistry* **100**, 88–95
17. Thompson, G. L., Roth, C., Tolstykh, G., Kuipers, M., and Ibey, B. L. (2014) Disruption of the actin cortex contributes to susceptibility of mammalian cells to nanosecond pulsed electric fields. *Bioelectromagnetics* **35**, 262–272
18. Carr, L., Bardet, S. M., Burke, R. C., Arnaud-Cormos, D., Leveque, P., and O'Connor, R. P. (2017) Calcium-independent disruption of microtubule dynamics by nanosecond pulsed electric fields in U87 human glioblastoma cells. *Sci. Rep.* **7**, 41267
19. Nesin, O. M., Pakhomova, O. N., Xiao, S., and Pakhomov, A. G. (2011) Manipulation of cell volume and membrane pore comparison following single cell permeabilization with 60- and 600-ns electric pulses. *Biochim. Biophys. Acta* **1808**, 792–801
20. Rassokhin, M. A., and Pakhomov, A. G. (2012) Electric field exposure triggers and guides formation of pseudopod-like blebs in U937 monocytes. *J. Membr. Biol.* **245**, 521–529

21. Rassokhin, M. A., and Pakhomov, A. G. (2014) Cellular regulation of extension and retraction of pseudopod-like blebs produced by nanosecond pulsed electric field (nsPEF). *Cell Biochem. Biophys.* **69**, 555–566
22. Nesin, V., Bowman, A. M., Xiao, S., and Pakhomov, A. G. (2012) Cell permeabilization and inhibition of voltage-gated Ca^{2+} and Na^{+} channel currents by nanosecond pulsed electric field. *Bioelectromagnetics* **33**, 394–404
23. Nesin, V., and Pakhomov, A. G. (2012) Inhibition of voltage-gated Na^{+} current by nanosecond pulsed electric field (nsPEF) is not mediated by Na^{+} influx or Ca^{2+} signaling. *Bioelectromagnetics* **33**, 443–451
24. Pakhomov, O. N., Gregory, B. W., Semenov, I., and Pakhomov, A. G. (2013) Two modes of cell death caused by exposure to nanosecond pulsed electric field. *PLoS ONE* **8**, e70278
25. Ren, W., and Beebe, S. J. (2011) An apoptosis targeted stimulus with nanosecond pulsed electric fields (nsPEFs) in E4 squamous cell carcinoma. *Apoptosis* **16**, 382–393
26. Gianulis, E. C., Labib, C., Saulis, G., Novickij, V., Pakhomova, O. N., and Pakhomov, A. G. (2017) Selective susceptibility to nanosecond pulsed electric field (nsPEF) across different human cell types. *Cell Mol. Life Sci.* **74**, 1741–1754
27. Berridge, M. J., Lipp, P., and Bootman, M. D. (2000) The versatility and universality of calcium signalling. *Nat. Rev. Mol. Cell Biol.* **1**, 11–21
28. Vernier, P. T., Sun, Y., Chen, M. T., Gundersen, M. A., and Craviso, G. L. (2008) Nanosecond electric pulse-induced calcium entry into chromaffin cells. *Bioelectrochemistry* **73**, 1–4
29. Craviso, G. L., Choe, S., Chatterjee, P., Chatterjee, I., and Vernier, P. T. (2010) Nanosecond electric pulses: a novel stimulus for triggering Ca^{2+} influx into chromaffin cells via voltage-gated Ca^{2+} channels. *Cell Mol. Neurobiol.* **30**, 1259–1265
30. Xiao, Q., Yu, K., Perez-Cornejo, P., Cui, Y., Arreola, J., and Hartzell, H. C. (2011) Voltage- and calcium-dependent gating of TMEM16A/Ano1 chloride channels are physically coupled by the first intracellular loop. *Proc. Natl. Acad. Sci. U.S.A.* **108**, 8891–8896
31. Hartzell, H. C., Yu, K., Xiao, Q., Chien, L. T., and Qu, Z. (2009) Anoctamin/TMEM16 family members are Ca^{2+} -activated Cl^{-} channels. *J. Physiol.* **587**, 2127–2139
32. Pedemonte, N., and Galletta, L. J. (2014) Structure and function of TMEM16 proteins (anoctamins). *Physiol. Rev.* **94**, 419–459
33. Suzuki, J., Umeda, M., Sims, P. J., and Nagata, S. (2010) Calcium-dependent phospholipid scrambling by TMEM16F. *Nature* **468**, 834–838
34. Castoldi, E., Collins, P. W., Williamson, P. L., and Bevers, E. M. (2011) Compound heterozygosity for 2 novel TMEM16F mutations in a patient with Scott syndrome. *Blood* **117**, 4399–4400
35. Munnix, I. C., Harmsma, M., Giddings, J. C., Collins, P. W., Feijge, M. A., Comfurios, P., Heemskerk, J. W., and Bevers, E. M. (2003) Store-mediated calcium entry in the regulation of phosphatidylserine exposure in blood cells from Scott patients. *Thromb. Haemost.* **89**, 687–695
36. Mattheij, N. J., Braun, A., van Kruchten, R., Castoldi, E., Pircher, J., Baaten, C. C., Wülling, M., Kuijpers, M. J., Köhler, R., Poole, A. W., Schreiber, R., Vortkamp, A., Collins, P. W., Nieswandt, B., Kunzelmann, K., Cosemanns, J. M., and Heemskerk, J. W. (2016) Survival protein anoctamin-6 controls multiple platelet responses including phospholipid scrambling, swelling, and protein cleavage. *FASEB J.* **30**, 727–737
37. Yang, H., Kim, A., David, T., Palmer, D., Jin, T., Tien, J., Huang, F., Cheng, T., Coughlin, S. R., Jan, Y. N., and Jan, L. Y. (2012) TMEM16F forms a Ca^{2+} -activated cation channel required for lipid scrambling in platelets during blood coagulation. *Cell* **151**, 111–122
38. Almaça, J., Tian, Y., Aldehni, F., Ousingsawat, J., Kongsuphol, P., Rock, J. R., Harfe, B. D., Schreiber, R., and Kunzelmann, K. (2009) TMEM16 proteins produce volume-regulated chloride currents that are reduced in mice lacking TMEM16A. *J. Biol. Chem.* **284**, 28571–28578
39. Martins, J. R., Faria, D., Kongsuphol, P., Reisch, B., Schreiber, R., and Kunzelmann, K. (2011) Anoctamin 6 is an essential component of the outwardly rectifying chloride channel. *Proc. Natl. Acad. Sci. U.S.A.* **108**, 18168–18172
40. Juul, C. A., Grubb, S., Poulsen, K. A., Kyed, T., Hashem, N., Lambert, I. H., Larsen, E. H., and Hoffmann, E. K. (2014) Anoctamin 6 differs from VRAC and VSOAC but is involved in apoptosis and supports volume regulation in the presence of Ca^{2+} . *Pflugers Arch.* **466**, 1899–1910
41. Shimizu, T., Iehara, T., Sato, K., Fujii, T., Sakai, H., and Okada, Y. (2013) TMEM16F is a component of a Ca^{2+} -activated Cl^{-} channel but not a volume-sensitive outwardly rectifying Cl^{-} channel. *Am. J. Physiol. Cell Physiol.* **304**, C748–759
42. Szteyn, K., Schmid, E., Nurbaeva, M. K., Yang, W., Münzer, P., Kunzelmann, K., Lang, F., and Shumilina, E. (2012) Expression and functional significance of the Ca^{2+} -activated Cl^{-} channel ANO6 in dendritic cells. *Cell Physiol. Biochem.* **30**, 1319–1332
43. Grubb, S., Poulsen, K. A., Juul, C. A., Kyed, T., Klausen, T. K., Larsen, E. H., and Hoffmann, E. K. (2013) TMEM16F (Anoctamin 6), an anion channel of delayed Ca^{2+} activation. *J. Gen. Physiol.* **141**, 585–600
44. Whitlock, J. M., and Hartzell, H. C. (2016) A pore idea: the ion conduction pathway of TMEM16/ANO proteins is composed partly of lipid. *Pflugers Arch.* **468**, 455–473
45. Shimizu, T., Numata, T., and Okada, Y. (2004) A role of reactive oxygen species in apoptotic activation of volume-sensitive Cl^{-} channel. *Proc. Natl. Acad. Sci. U.S.A.* **101**, 6770–6773
46. Vernier, P. T., Sun, Y., Marcu, L., Craft, C. M., and Gundersen, M. A. (2004) Nanosecond pulsed electric fields perturb membrane phospholipids in T lymphoblasts. *FEBS Lett.* **572**, 103–108
47. Suzuki, T., Suzuki, J., and Nagata, S. (2014) Functional swapping between transmembrane proteins TMEM16A and TMEM16F. *J. Biol. Chem.* **289**, 7438–7447
48. Ousingsawat, J., Wanitchakool, P., Kmit, A., Romao, A. M., Jantarajit, W., Schreiber, R., and Kunzelmann, K. (2015) Anoctamin 6 mediates effects essential for innate immunity downstream of P2X7 receptors in macrophages. *Nat. Commun.* **6**, 6245
49. Craviso, G. L., Choe, S., Chatterjee, I., and Vernier, P. T. (2012) Modulation of intracellular Ca^{2+} levels in chromaffin cells by nanoelectropulses. *Bioelectrochemistry* **87**, 244–252
50. Vernier, P. T., Sun, Y., Marcu, L., Salemi, S., Craft, C. M., and Gundersen, M. A. (2003) Calcium bursts induced by nanosecond electric pulses. *Biochem. Biophys. Res. Commun.* **310**, 286–295
51. Jewell, S. A., Bellomo, G., Thor, H., Orrenius, S., and Smith, M. (1982) Bleb formation in hepatocytes during drug metabolism is caused by disturbances in thiol and calcium ion homeostasis. *Science* **217**, 1257–1259
52. Arnould, T., Michiels, C., Alexandre, L., and Remacle, J. (1992) Effect of hypoxia upon intracellular calcium concentration of human endothelial cells. *J. Cell Physiol.* **152**, 215–221
53. Geeraerts, M. D., Ronveaux-Dupal, M. F., Lemasters, J. J., and Herman, B. (1991) Cytosolic free Ca^{2+} and proteolysis in lethal oxidative injury in endothelial cells. *Am. J. Physiol.* **261**, C889–896
54. Tsien, R. Y. (1980) New calcium indicators and buffers with high selectivity against magnesium and protons: design, synthesis, and properties of prototype structures. *Biochemistry* **19**, 2396–2404
55. Ren, W., Sain, N. M., and Beebe, S. J. (2012) Nanosecond pulsed electric fields (nsPEFs) activate intrinsic caspase-dependent and caspase-independent cell death in Jurkat cells. *Biochem. Biophys. Res. Commun.* **421**, 808–812
56. Garon, E. B., Sawcer, D., Vernier, P. T., Tang, T., Sun, Y., Marcu, L., Gundersen, M. A., and Koeffler, H. P. (2007) In vitro and in vivo evaluation and a case report of intense nanosecond pulsed electric field as a local therapy for human malignancies. *Int. J. Cancer* **121**, 675–682
57. Yang, W., Wu, Y. H., Yin, D., Koeffler, H. P., Sawcer, D. E., Vernier, P. T., and Gundersen, M. A. (2011) Differential sensitivities of malignant and normal skin cells to nanosecond pulsed electric fields. *Technol. Cancer Res. Treat.* **10**, 281–286
58. Ibey, B. L., Pakhomov, A. G., Gregory, B. W., Khorokhorina, V. A., Roth, C. C., Rassokhin, M. A., Bernhard, J. A., Wilmink, G. J., and Pakhomova, O. N. (2010) Selective cytotoxicity of intense nanosecond-duration electric pulses in mammalian cells. *Biochim. Biophys. Acta* **1800**, 1210–1219
59. Taylor, R. C., Cullen, S. P., and Martin, S. J. (2008) Apoptosis: controlled demolition at the cellular level. *Nat. Rev. Mol. Cell Biol.* **9**, 231–241
60. Matorini, C., Pakhomov, A. G., and Pakhomova, O. N. (2017) Effect of cooling on cell volume and viability after nanoelectroporation. *J. Membr. Biol.* **250**, 217–224

61. Kunzelmann, K., Nilius, B., Owsianik, G., Schreiber, R., Ousingsawat, J., Sirianant, L., Wanitchakool, P., Bevers, E. M., and Heemskerk, J. W. (2014) Molecular functions of anoctamin 6 (TMEM16F): a chloride channel, cation channel, or phospholipid scramblase? *Pflugers Arch.* **466**, 407–414
62. Vernier, P. T., Ziegler, M. J., Sun, Y., Chang, W. V., Gundersen, M. A., and Tieleman, D. P. (2006) Nanopore formation and phosphatidylserine externalization in a phospholipid bilayer at high transmembrane potential. *J. Am. Chem. Soc.* **128**, 6288–6289
63. Vernier, P. T., Ziegler, M. J., Sun, Y., Gundersen, M. A., and Tieleman, D. P. (2006) Nanopore-facilitated, voltage-driven phosphatidylserine translocation in lipid bilayers: in cells and *in silico*. *Phys. Biol.* **3**, 233–247
64. Hu, Q., Joshi, R. P., and Schoenbach, K. H. (2005) Simulations of nanopore formation and phosphatidylserine externalization in lipid membranes subjected to a high-intensity, ultrashort electric pulse. *Phys. Rev. E Stat. Nonlin. Soft Matter Phys.* **72**, 031902
65. Pakhomova, O. N., Gregory, B., Semenov, I., and Pakhomov, A. G. (2014) Calcium-mediated pore expansion and cell death following nanoelectroporation. *Biochim. Biophys. Acta* **1838**, 2547–2554
66. Charras, G. T. (2008) A short history of blebbing. *J. Microsc.* **231**, 466–478
67. Blaser, H., Reichman-Fried, M., Castanon, I., Dumstrei, K., Marlow, F. L., Kawakami, K., Solnica-Krezel, L., Heisenberg, C. P., and Raz, E. (2006) Migration of zebrafish primordial germ cells: a role for myosin contraction and cytoplasmic flow. *Dev. Cell* **11**, 613–627
68. Pletjushkina, O. J., Rajfur, Z., Pomorski, P., Oliver, T. N., Vasiliev, J. M., and Jacobson, K. A. (2001) Induction of cortical oscillations in spreading cells by depolymerization of microtubules. *Cell Motil. Cytoskeleton* **48**, 235–244
69. Scudieri, P., Caci, E., Venturini, A., Sondo, E., Pianigiani, G., Marchetti, C., Ravazzolo, R., Pagani, F., and Galletta, L. J. (2015) Ion channel and lipid scramblase activity associated with expression of TMEM16F/ANO6 isoforms. *J. Physiol.* **593**, 3829–3848
70. Semenov, I., Xiao, S., Kang, D., Schoenbach, K. H., and Pakhomov, A. G. (2015) Cell stimulation and calcium mobilization by picosecond electric pulses. *Bioelectrochemistry* **105**, 65–71
71. Jiang, N., and Cooper, B. Y. (2011) Frequency-dependent interaction of ultrashort E-fields with nociceptor membranes and proteins. *Bioelectromagnetics* **32**, 148–163
72. Wang, S., Chen, J., Chen, M. T., Vernier, P. T., Gundersen, M. A., and Valderrábano, M. (2009) Cardiac myocyte excitation by ultrashort high-field pulses. *Biophys. J.* **96**, 1640–1648
73. Pakhomov, A. G., Semenov, I., Casciola, M., and Xiao, S. (2017) Neuronal excitation and permeabilization by 200-ns pulsed electric field: An optical membrane potential study with FluoVolt dye. *Biochim. Biophys. Acta* **1859**, 1273–1281
74. Kunzelmann, K. (2016) Ion channels in regulated cell death. *Cell Mol. Life Sci.* **73**, 2387–2403
75. Ullery, J. C., Tarango, M., Roth, C. C., and Ibey, B. L. (2015) Activation of autophagy in response to nanosecond pulsed electric field exposure. *Biochem. Biophys. Res. Commun.* **458**, 411–417
76. Ousingsawat, J., Cabrita, I., Wanitchakool, P., Sirianant, L., Krautwald, S., Linkermann, A., Schreiber, R., and Kunzelmann, K. (2017) Ca²⁺ signals, cell membrane disintegration, and activation of TMEM16F during necroptosis. *Cell Mol. Life Sci.* **74**, 173–181
77. Muratori, C., Pakhomov, A. G., Xiao, S., and Pakhomova, O. N. (2016) Electrosensitization assists cell ablation by nanosecond pulsed electric field in 3D cultures. *Sci. Rep.* **6**, 23225
78. Pakhomov, A. G., Gianulis, E., Vernier, P. T., Semenov, I., Xiao, S., and Pakhomova, O. N. (2015) Multiple nanosecond electric pulses increase the number but not the size of long-lived nanopores in the cell membrane. *Biochim. Biophys. Acta* **1848**, 958–966
79. Ibey, B. L., Mixon, D. G., Payne, J. A., Bowman, A., Sickendick, K., Wilimink, G. J., Roach, W. P., and Pakhomov, A. G. (2010) Plasma membrane permeabilization by trains of ultrashort electric pulses. *Bioelectrochemistry* **79**, 114–121
80. Yu, K., Whitlock, J. M., Lee, K., Ortlund, E. A., Cui, Y. Y., and Hartzell, H. C. (2015) Identification of a lipid scrambling domain in ANO6/TMEM16F. *Elife* **4**, e06901
81. Muratori, C., Pakhomov, A. G., Gianulis, E. C., Jensen, S. D., and Pakhomova, O. N. (2016) The cytotoxic synergy of nanosecond electric pulses and low temperature leads to apoptosis. *Sci. Rep.* **6**, 36835

Activation of the phospholipid scramblase TMEM16F by nanosecond pulsed electric fields (nsPEF) facilitates its diverse cytophysiological effects
Claudia Muratori, Andrei G. Pakhomov, Elena Gianulis, Jade Meads, Maura Casciola,
Peter A. Mollica and Olga N. Pakhomova

J. Biol. Chem. 2017, 292:19381-19391.

doi: 10.1074/jbc.M117.803049 originally published online October 5, 2017

Access the most updated version of this article at doi: [10.1074/jbc.M117.803049](https://doi.org/10.1074/jbc.M117.803049)

Alerts:

- [When this article is cited](#)
- [When a correction for this article is posted](#)

[Click here](#) to choose from all of JBC's e-mail alerts

This article cites 79 references, 11 of which can be accessed free at <http://www.jbc.org/content/292/47/19381.full.html#ref-list-1>